

# Frequency-resolved coherent lidar using a femtosecond fiber laser

W. C. Swann and N. R. Newbury

National Institute of Standards and Technology, 325 Broadway, Boulder, Colorado 80305

Received September 22, 2005; accepted November 7, 2005; posted November 23, 2005 (Doc. ID 64945)

We demonstrate a coherent lidar that uses a broadband femtosecond fiber laser as a source and resolves the returning heterodyne signal into  $N$  spectral channels by using an arrayed-waveguide grating. The data are processed incoherently to yield an  $N$ -times improvement in the Doppler measurement of a surface vibration. For  $N=6$ , we achieve a sensitivity of 153 Hz, corresponding to a 0.12 mm/s motion, in 10 ms despite a signal that is speckle broadened to 14 kHz. Alternatively, the data are processed coherently to form a range image. For a flat target, we achieve a 60  $\mu\text{m}$  range resolution, limited mainly by the source bandwidth, despite the dispersion of 1 km of optical fiber in the signal path. © 2006 Optical Society of America

OCIS codes: 140.3510, 280.3640, 120.0280.

In recent years mode-locked femtosecond lasers have been shown to produce highly coherent output. These sources emit a broad spectrum of light that comprises a set of narrow individual optical lines in frequency space separated by the laser repetition rate, i.e., a frequency comb. Frequency combs have revolutionized optical frequency metrology.<sup>1</sup> It is natural to extend their use to coherent light detection and ranging (Clidar) for range or Doppler measurements,<sup>2</sup> since the broad spectrum supports high range resolution and the narrow linewidth of each comb tooth supports high Doppler resolution. Fiber-laser-based frequency combs<sup>3,4</sup> at 1.5  $\mu\text{m}$  are compatible with high-power erbium-doped fiber amplifiers (EDFAs). Furthermore, free-running fiber-laser combs have linewidths of <4 kHz, sufficient for ranges of tens of kilometers, and phase-locked systems could potentially exhibit narrower linewidths.<sup>5</sup> Indeed, frequency combs have been employed in a ranging lidar for several years<sup>6</sup> and have been proposed for measuring absolute distance in space.<sup>7</sup>

In pulsed coherent lidar, a pulse of laser light is amplified and diffusely reflected from a remote rough surface.<sup>8,9</sup> The received reflection is mixed with a local oscillator (LO), typically a delayed and RF-shifted copy of the original transmitted pulse, to generate a heterodyne signal. By recording the amplitude of the heterodyne signal as a function of LO delay, a range image of the surface is generated. By measuring the frequency shift of the heterodyne signal, a velocity, i.e. vibrational, signature of the surface is generated. Using a femtosecond fiber laser as a source for coherent lidar presents several challenges. First, as with any coherent lidar, the return signal suffers from speckle,<sup>10</sup> which limits the signal-to-noise ratio (SNR) to unity regardless of the transmitted power. It also broadens the frequency spectrum to the speckle bandwidth, which is inversely proportional to the time for a speckle lobe to cross the receive aperture, thereby making the measurement of small Doppler shifts much more difficult. Second, the wide source bandwidth permits fine range resolution, but only if the LO delay is adjustable over very fine increments. For our 25 nm source bandwidth the LO must arrive within 300 fs of the signal, regardless of the relative motion between the source and the sur-

face. Third, unbalanced dispersion in the signal and LO paths can drastically degrade the range resolution, particularly for a wide-bandwidth source. (A final issue of high-power chirped pulse amplification<sup>11</sup> is not considered here.)

To effectively deal with these issues, we demonstrate a frequency-resolved coherent lidar (FReCL) in which the heterodyne signal is spectrally resolved into  $N$  channels by using an arrayed waveguide grating (AWG). The data can be processed incoherently to produce a vibration profile or coherently to produce a range image. In either case, this system has a performance  $N$ -times superior to a single-channel, conventional Clidar and removes the tight requirements on the delay line. Our system differs significantly from previous comb-based lidars<sup>6,7</sup> and shares features of spectrally diverse Clidars<sup>12,13</sup> and Fourier-domain optical coherence tomography<sup>14</sup> (FDOCT). As with spectrally diverse Clidars, the Doppler (vibrometry) return is improved by averaging over the  $N$  spectral channels; provided the target's range depth is sufficiently large, these channels are uncorrelated, reducing the measurement's variance by a factor of  $N$ . Previous spectrally diverse Clidars used either two narrowly spaced modes of a multimode cw laser<sup>12</sup> or two distinct cw lasers<sup>13</sup>; the single femtosecond laser represents a convenient, compact source that can

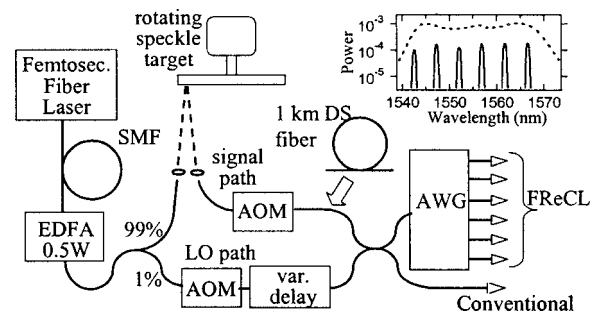


Fig. 1. System layout. Solid curves are fiber paths, dotted lines are air paths. The variable delay line precisely adjusts the relative delay between the two arms and permits scanning the conventional lidar's range. AOM, acousto-optic modulator; EDFA, erbium-doped fiber amplifier; SMF, 800 m of single-mode fiber. Inset, output spectrum of the amplified source (dashed curve) and the individual spectra of the filtered FReCL channels (solid curves).

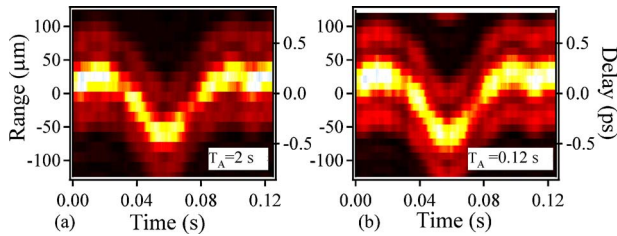


Fig. 2. (Color online) Relative range image of the wobbling, rotating disk for one full rotation (0.12 s) for balanced signal and LO arms with a 10 ms averaging time. The range image from the conventional channel shown in (a) is acquired by accumulating the response over 17 disk revolutions. (In one disk revolution, only one horizontal stripe of data is obtained.) (b) Alternatively, in one disk revolution the FReCL data yield the entire range image. Identical FReCL images can be obtained at other delays.  $T_A$  is the total acquisition time.

provide a large number of coherent modes. We achieve a Doppler sensitivity of  $\pm 153$  Hz (0.12 mm/s) at a 10 ms averaging time for our  $N=6$  channels, despite a return signal speckle broadened to 14 kHz FWHM. Higher channel numbers would further improve the Doppler sensitivity. As with FdOCT, the range image is generated as the Fourier transform of the  $N$  detected channels after any necessary phase compensation for signal path dispersion and does not require a precisely adjustable delay line. Here we achieve a range resolution of  $60 \mu\text{m}$  FWHM after phase compensation despite the extra dispersion from 1 km of optical fiber (corresponding to an  $\sim 10$  km air path), a 20-fold improvement over the uncompensated image's resolution and only 25% larger than the  $48 \mu\text{m}$  FWHM resolution imposed by the 25 nm source bandwidth. Our range ambiguity is  $250 \mu\text{m}$ ; however, higher channel numbers would support larger range ambiguities.

Figure 1 shows the basic setup for our demonstration lidar. The free-running femtosecond fiber laser has a 50 MHz repetition rate and individual comb linewidths of  $<4$  kHz as measured against a separate narrow-linewidth CW fiber laser. The output was preamplified, stretched in time, and spectrally broadened to  $\lambda_{\text{BW}}=25$  nm in single-mode fiber, then amplified to 0.5 W. The stretching is common mode to the signal and LO and, as such, does not reduce the range resolution. The beam was collimated to an  $\sim 3$  mm diameter and reflected from a rough target rotating at about 10 Hz, resulting in dynamic speckle that broadens the return signal to a linewidth of between 2 and 15 kHz FWHM, depending on target tilt.<sup>10</sup> The detected signal was combined with the pulse from the LO arm, which was set equal in length to the signal arm, modulo the laser repetition rate of 50 MHz. (Alternatively, a second phase-locked fiber comb can serve as a phase-locked LO to remove this restriction.<sup>15</sup>) The combined signal was split and one branch sent to a photodetector that served as the conventional pulsed-Doppler channel. The second branch passed through an AWG to  $N=6$  discrete detectors to provide the FReCL channels. The channels each had a bandwidth of  $\lambda_{\text{AWG}}=0.65$  nm and were spaced by  $\lambda_{\text{sp}}=4.8$  nm to sparsely cover the output

spectrum (see Fig. 1). For additive noise, this  $N$ -times division of the signal would degrade the overall SNR; however, for multiplicative speckle noise the SNR for each channel remains unity. The AOMs were offset to generate a heterodyne signal at  $\sim 30$  kHz. The total loss in the unoptimized signal path was  $\sim 69$  dB, with losses of 2, 60, and 7 dB from the AOM, air path, and AWG, respectively.

To demonstrate ranging capabilities, the rotating disk was set normal to the transmit beam, giving a small instantaneous range depth; however, its range varied by  $\sim 100 \mu\text{m}$  over one rotation as a result of wobble (confirmed with a mechanical measurement). Figure 2(a) shows the truth range image from the conventional channel. It was constructed by stacking the return strength as a function of rotation angle over 17 individual delays spaced by 0.1 ps ( $15 \mu\text{m}$ ) steps and exhibits a resolution of  $44 \mu\text{m}$  FWHM, commensurate with a 27 nm source bandwidth. Figure 2(b) shows the range image generated by a Fourier transform of the  $N=6$  channel FReCL data acquired at a single delay line position. As expected, the range resolution is  $\lambda^2/(2\lambda_{\text{BW}})=48 \mu\text{m}$ , commensurate with the 25 nm bandwidth spanned by the six channels. The unambiguous range window (equivalent to a Nyquist range) is set by the channel spacing as  $\lambda^2/(2\lambda_{\text{sp}})\sim 250 \mu\text{m}$ . In Fig. 2(b), zero padding prior to the Fourier transform gives finer range bins. In both images a slight echo is seen, presumably due to satellite pulses around the main pulse and, for Fig. 2(b), to the square apodization used. Range changes larger than the Nyquist range (i.e., a larger target wobble) could be tracked by unwrapping until the range change exceeds  $\lambda^2/(2\lambda_{\text{AWG}})\sim 1.8$  mm, at which point the delay line could be adjusted. For a target with a larger instantaneous range depth one could increase the Nyquist range by decreasing the channel spacing  $\lambda_{\text{sp}}$  by increasing  $N$  or decreasing  $\lambda_{\text{BW}}$ . Alternatively, one could oversample by choosing  $\lambda_{\text{sp}}\leq 0.7\lambda_{\text{AWG}}$ , to suppress the aliasing effect by 10 times or more. A complete range image would be obtained by stitching together FReCL range images taken at coarsely stepped delays. Uneven sparse sampling may also be an option.

Figure 3 shows a similar data set with the signal path increased using 1 km of fiber. The conventional channel's resolution is destroyed by the extra dispersion in the signal path [Fig. 3(a)]. However, adjusting the phase of the FReCL signals in software to com-

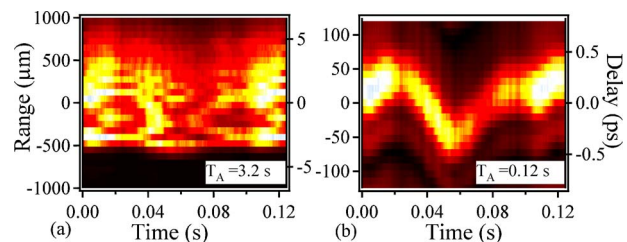


Fig. 3. (Color online) Range image of the same disk as Fig. 1, with 1 km of fiber in the signal path for (a) conventional data at 27 delay steps of 0.5 ps each and for (b) FReCL data at a fixed LO delay after phase compensation. Note the  $\sim 10\times$  larger range scale in (a) versus (b).

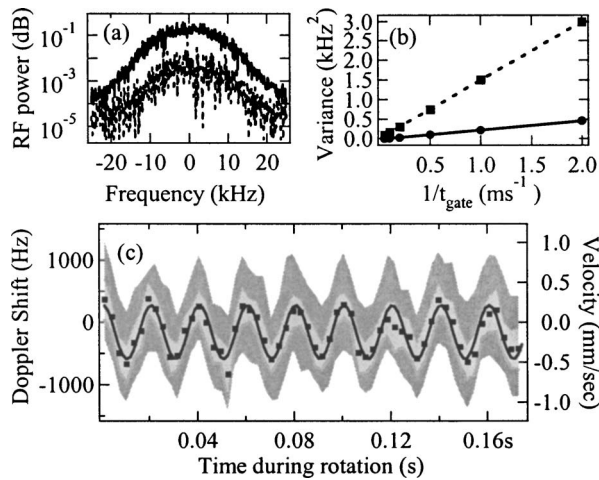


Fig. 4. (a) Example power spectrum: conventional (dashed curve) and FReCL data (solid curve) for  $t_{\text{gate}}=10$  ms. (b) Variance versus  $1/t_{\text{gate}}$  for the conventional (dashed line) and FReCL data (solid line). (c) Example vibration measurement. The mean of the FReCL channel measurements (filled squares) are in good agreement with the applied vibration (solid line) after adding  $\sim 100$  Hz shift from a small average longitudinal target velocity. For a single measurement (one target rotation), the standard deviation for the summed FReCL data is 280 Hz (light gray region) and for the single conventional channel is 700 Hz (dark gray region) for  $t_{\text{gate}}=3$  ms.

compensate for a second- and third-order dispersion<sup>14</sup> of  $0.15 \text{ ps}^2$  and  $0.0048 \text{ ps}^3$  gives a resolution of  $60 \mu\text{m}$  [Fig. 3(b)], only 25% degraded from the bandwidth-limited resolution of  $48 \mu\text{m}$ . In air, this corresponds to phase correction over a 10 km range.

Next we consider the velocity or vibration profile of the target. This was generated by applying a rectangular time window to the data with a gate time  $t_{\text{gate}}$ , Fourier transforming these data to produce a power spectrum, and finally estimating the Doppler shift by using Lee's algorithm,<sup>16</sup> e.g., a short-time Fourier transform technique. For the normally oriented target, the FReCL channels are fully correlated, yielding the same variance as the conventional channel. To decorrelate the channels, we increased the range depth to  $\sim 800 \mu\text{m}$  by tilting the target at  $15^\circ$  (retaining the 1 km fiber delay).<sup>12,13</sup> In addition, the wobble was reduced to remove the systematic target motion. Figure 4(a) also shows the power spectrum of the conventional channel. It is Gaussian shaped, with a speckle-broadened FWHM of 14 kHz.<sup>10,16</sup> Speckle limits each resolved frequency bin to an  $\text{SNR}=1$ , a consequence of the exponential (or Rayleigh) statistics. Figure 4(a) also shows the normalized, summed power spectrum for the FReCL data with an  $\text{SNR}=1/N$  per bin.

To demonstrate the improved Doppler shift measurement, we performed multiple measurements and compared the variance of the conventional and FReCL channels. 120 independent speckle realizations were generated by varying the target tilt angle from  $14.5^\circ$  to  $15.5^\circ$  in  $0.05^\circ$  increments and the delay over six positions in 0.3 ps increments. Figure 4(b) shows the comparison. For both, the variance increases as  $1/t_{\text{gate}}$  as expected for the incoherent addi-

tion of different speckle lobes. For  $t_{\text{gate}}=10$  ms, the statistical variance of the conventional channel is  $(384 \text{ Hz})^2$  and of the FReCL channels is  $(153 \text{ Hz})^2$ , or  $N=6$  times smaller. (These values are  $\sim 3\times$  the Cramer-Rao lower bound.<sup>16</sup>) The wideband SNR is  $\sim 15\text{--}20$  dB; simulations indicate that the sixfold advantage should remain down to  $\sim 0$  dB. Finally, to demonstrate a vibration measurement, we inserted a fiber stretcher in the signal path and applied a sinusoidal voltage to mimic a target vibration at 50 Hz with a peak velocity of 0.34 mm/s (440 Hz Doppler shift). Figure 4(c) compares the measured and applied 50 Hz vibration; only the FReCL measurement can effectively resolve the vibration.

Here we have demonstrated that the use of a broadband coherent source and frequency-resolved detection can permit  $N$ -times performance improvement over a conventional lidar system for either range images or Doppler vibration measurements, depending on the system configuration and the instantaneous target range depth, and provided the SNR is speckle limited at unity. The optimal choice of channel width, channel spacing, and overall spectral width will depend on the application; we have demonstrated one possible configuration here that is compatible with laboratory-based measurements.

N. R. Newbury's e-mail address is [nnewbury@boulder.nist.gov](mailto:nnewbury@boulder.nist.gov).

## References

1. S. A. Diddams, D. J. Jones, S. T. C. J. Ye, J. L. Hall, J. K. Ranka, R. S. Windeler, R. Holzwarth, T. Udem, and T. W. Hänsch, *Phys. Rev. Lett.* **84**, 5102 (2000).
2. R. M. Huffaker and R. M. Hardesty, *Proc. IEEE* **84**, 181 (1996).
3. B. R. Washburn, S. A. Diddams, N. R. Newbury, J. W. Nicholson, M. F. Yan, and C. G. Jørgensen, *Opt. Lett.* **29**, 250 (2004).
4. T. R. Schibli, K. Minoshima, F.-L. Hong, H. Inaba, A. Onae, H. Matsumoto, I. Hartl, and M. N. Fermann, *Opt. Lett.* **29**, 2467 (2004).
5. A. Bartels, C. W. Oates, L. Hollberg, and S. A. Diddams, *Opt. Lett.* **29**, 1081 (2004).
6. K. Minoshima and H. Matsumoto, *Appl. Opt.* **39**, 5512 (2000).
7. J. Ye, *Opt. Lett.* **29**, 1153 (2004).
8. G. N. Pearson, J. Roberts, J. R. Eacock, and M. Harris, *Appl. Opt.* **41**, 6442 (2002).
9. C. J. Karlsson, F. A. A. Olsson, D. Letalick, and M. Harris, *Appl. Opt.* **39**, 3716 (2000).
10. D. Letalick, I. Renhorn, O. Steinvall, and J. H. Shapiro, *Appl. Opt.* **28**, 2657 (1989).
11. V. Philippov, C. Codemard, Y. Jeong, C. Alegria, J. Sahu, J. Nilsson, and G. N. Pearson, *Opt. Lett.* **29**, 2590 (2004).
12. P. Drobninski, P. H. Flamant, P. Salamitou, *Appl. Opt.* **39**, 376 (2000).
13. K. D. Ridley, G. N. Pearson, and M. Harris, *Appl. Opt.* **40**, 2017 (2001).
14. M. Wojtkowski, V. J. Srinivasan, T. H. Ko, J. G. Fujimoto, A. Kowalczyk, and J. S. Duker, *Opt. Express* **12**, 2404-2422 (2004).
15. B. R. Washburn, R. Fox, N. R. Newbury, J. W. Nicholson, K. Feder, P. S. Westbrook, and C. G. Jørgensen, *Opt. Express* **12**, 4999 (2004).
16. B. J. Rye, and R. M. Hardesty, *IEEE Trans. Geosci. Remote Sens.* **31**, 16 (1993).